

Exploring lasing modes and polarization characteristics in broad-area square-shaped vertical-cavity surface emitting lasers with frequency detuning

This content has been downloaded from IOPscience. Please scroll down to see the full text.

2014 Laser Phys. Lett. 11 115001

(<http://iopscience.iop.org/1612-202X/11/11/115001>)

View [the table of contents for this issue](#), or go to the [journal homepage](#) for more

Download details:

IP Address: 140.113.38.11

This content was downloaded on 21/07/2015 at 10:00

Please note that [terms and conditions apply](#).

Exploring lasing modes and polarization characteristics in broad-area square-shaped vertical-cavity surface emitting lasers with frequency detuning

Y T Yu, P H Tuan, C P Wen, K F Huang and Y F Chen

Department of Electrophysics, National Chiao Tung University, 1001 Ta-Huseh Road, Hsinchu, 30050, Taiwan

E-mail: yfchen@cc.nctu.edu.tw

Received 23 August 2013, revised 15 August 2014

Accepted for publication 18 August 2014

Published 22 September 2014

Abstract

We experimentally explore the polarization characteristics of broad-area square-shaped vertical-cavity surface emitting lasers with the cryogenic cooling to achieve a wide range of frequency detuning. At room temperature the lasing modes are subject to thermal effects and exhibit the phenomenon of polarization switching. For operating temperatures below 260 K, the transverse modes are confirmed to be mainly controlled by the lateral oxide boundary and usually do not display polarization switching. Near the maximum frequency detuning, the lasing modes are well localized on the ray trajectories and display a remarkable frequency-locking phenomenon from single-frequency to multi-frequency operation for the injected current changing from near to far above lasing threshold.

Keywords: vertical-cavity surface emitting laser, transverse modes, polarization dynamics, frequency detuning

(Some figures may appear in colour only in the online journal)

1. Introduction

Vertical-cavity surface emitting lasers (VCSELs) have been identified as a charming light source for a variety of practical applications such as optical communications, data transmissions, high-density optical storages and optical sensors [1–4]. One of the challenges of the use of VCSELs is the polarization instability that mainly comes from competition between two orthogonally polarized modes. The mode competition is primarily associated with the spatial overlap of the net gains for two orthogonally polarized modes. Without introducing intentional anisotropies, the difference between the net gains of two orthogonally polarized modes is usually not considerable [5–8]. Under this circumstance, varying injection current may lead to the dominant lasing mode switching from some polarized state to another orthogonally polarized state [9–14]. In the vicinity of the switching point, the output amplitudes of two orthogonally polarized modes are found to significantly

display the anti-phase dynamics. The phenomenon of polarization switching widely exists in most VCSELs and several efforts have been proposed for generating light emission without polarization switching, such as optical feedback [15, 16], applying in-plane strain [17], and introducing large-cavity anisotropy into the VCSEL [18–21].

So far, the polarization dynamics of oxide-confined VCSELs has been mostly concentrated on studying small-aperture devices with active areas smaller than $15 \times 15 \mu\text{m}^2$. Only few low-order transverse modes can be generated in the small-aperture devices. In contrast, numerous high-order transverse modes can be generated in the large-aperture VCSELs with active areas greater than $25 \times 25 \mu\text{m}^2$. Intriguingly, the transverse order in the large-aperture devices can be so high that the spatial morphologies of the lasing modes may be well localized on the geometric trajectories to exhibit the ray-wave duality [22–24]. More recently, investigation of square-shaped VCSELs revealed that the polarization directions of the lasing

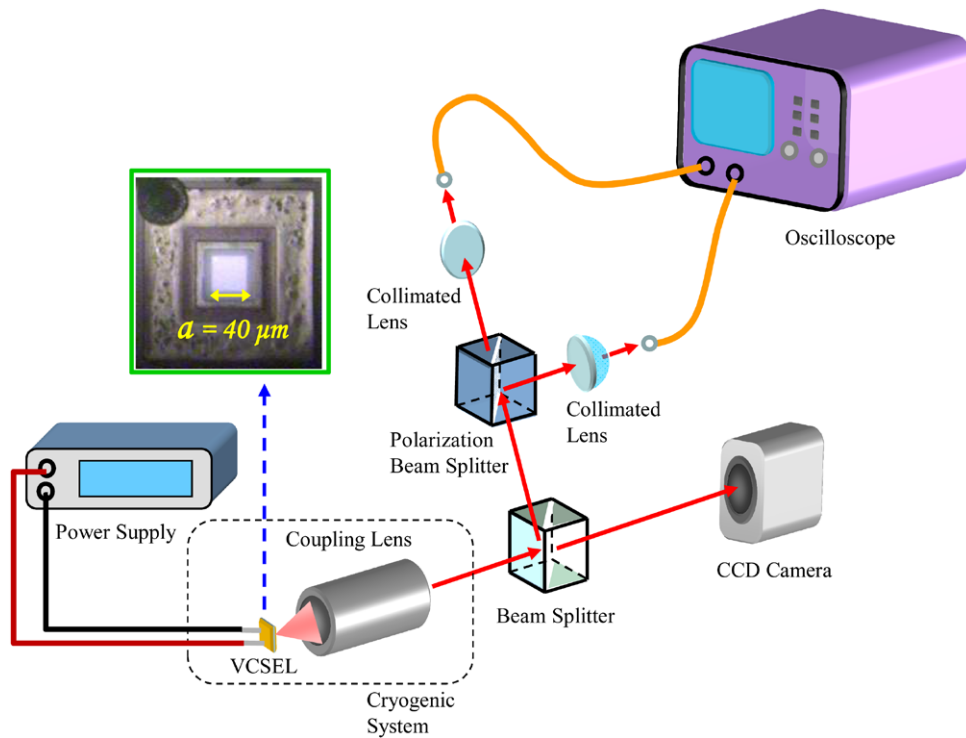


Figure 1. Schematic diagram of the VCSEL devices and the experimental set-up.

modes with ray-wave duality were deeply related to their spatial morphologies [25]. Due to the notable difference in the pattern formation of lasing modes, the scenario of the polarization dynamics in the large-aperture VCSELs should be significantly different from that for the small-aperture VCSELs. Nevertheless, the exploration of the polarization dynamics of the large-aperture VCSELs has not been performed yet.

The transverse order of the lasing mode in VCSELs is primarily determined by the frequency detuning $\Delta\omega = \omega - \omega_c$, where ω is the central frequency of the gain profile and ω_c is the frequency of the fundamental cavity mode. In this work, we exploit cryogenic cooling to achieve a wide range of frequency detuning for exploring the polarization characteristics of broad-area square-shaped VCSELs. The initial frequency detuning of the device at room temperature is designed to be approximately 1.26 THz. The maximum frequency detuning can be up to 32 THz at the operating temperature of 190 K and the limitation chiefly comes from the effective optical confinement of the lateral oxide. At room temperature the transverse patterns of the lasing modes are found to be virtually subject to the thermal effects. Experimental results reveal that there are numerous abrupt changes (kinks) in the light-current curves (L-I curves) of the two orthogonal polarizations. Near the kinks in the L-I curves, the time traces are found to display the characteristic of the anti-phase oscillation. Furthermore, the high-resolution optical spectra clearly show the mode competition and the frequency splitting between the two orthogonal polarizations. For operating temperatures below 260 K, the transverse modes are confirmed to be mainly associated with lateral oxide confinement. Under the boundary-controlled regime, there are no conspicuous kinks in the polarization-resolved L-I curves and no polarization switching is observed in the time traces.

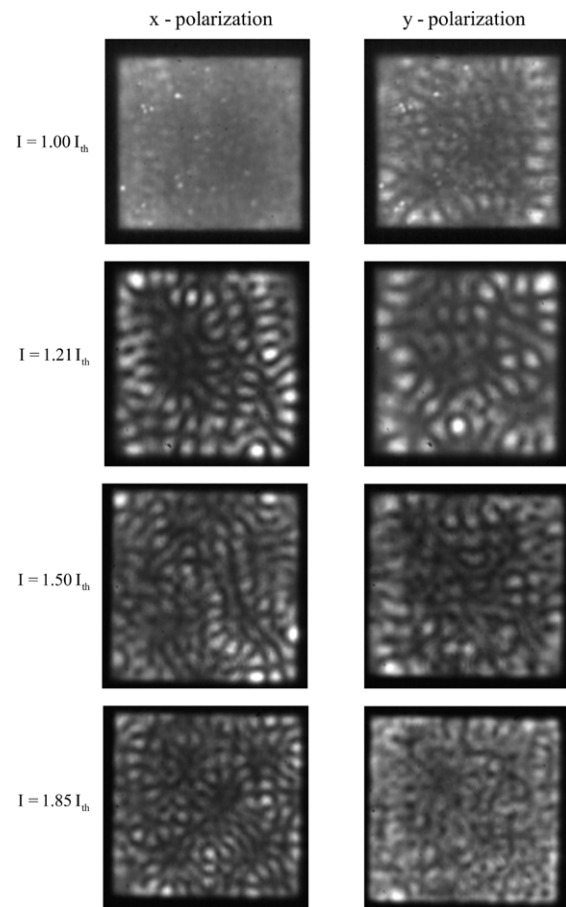


Figure 2. Polarization resolved near-field pattern at the injected currents of $1.0 I_{th}$, $1.21 I_{th}$, $1.50 I_{th}$ and $1.85 I_{th}$.

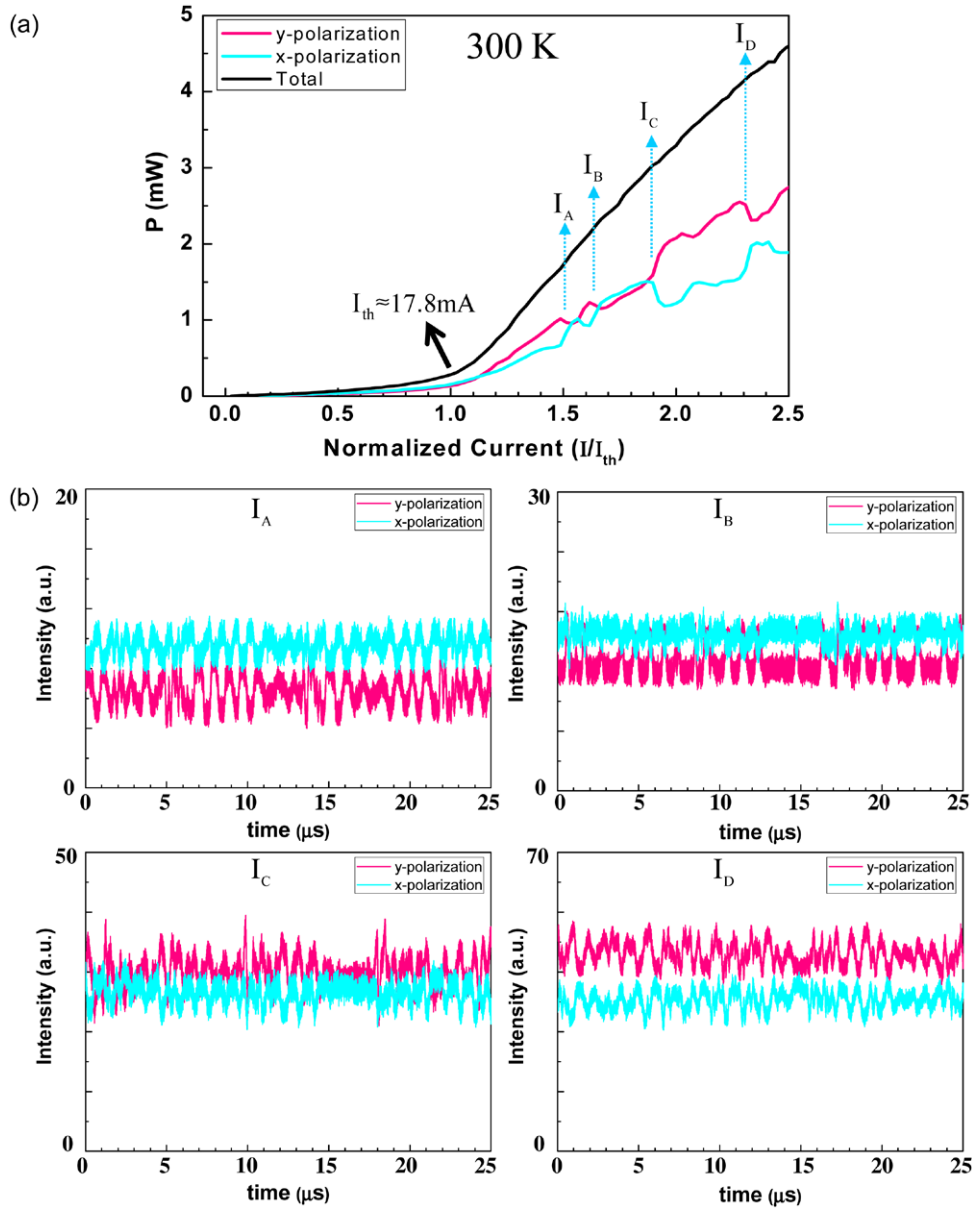


Figure 3. (a) The L-I curve for the square-shaped VCSEL at room temperature. (b) Intensity time trace of the two orthogonal polarized states at the kinks of the L-I curve.

In the range of 220 K and 260 K, the transverse patterns of the lasing modes generally exhibit a feature of the quasi-periodic linear ridges, and the polarization directions are found to be perpendicular to the ridge structure. Thanks to the orthogonal property of the linear ridges, the mode competition between both polarization components can be effectively avoided so as not to cause polarization switching. For operating temperatures below 200 K, the lasing patterns are well localized on the ray trajectories of the diamond orbit. More remarkably, the polarization-resolved optical spectra reveal that the two orthogonally polarized modes are persistently locked in the same spectral components from single-frequency to multi-frequency operation, corresponding to the injected current varying from near to far above lasing threshold. The total frequency locking between two orthogonally polarized modes leads the broad-area squared-shaped VCSEL to be resistant to polarization switching.

2. Experimental set-up

Figure 1 illustrates a schematic diagram of the VCSEL devices and the experimental set-up. The aperture size of the square-shaped VCSEL was approximately $40 \times 40 \mu\text{m}^2$. The device structure of the oxide-confined VCSEL was similar to those described in [26]. The emission wavelength of the VCSEL was approximately 800 nm. The VCSEL device was placed in a cryogenic system with a temperature stability of 0.1 K in the range of 180 – 300 K. A power supply providing a current with a precision of 0.01 mA was utilized to drive the VCSEL. The laser output was collimated by an objective lens (Mitutoyo, numerical aperture 0.9) and is divided into two parts of lights with equal intensities by a beam splitter (BS). One part of the light was coupled into a charge-coupled device (CCD) camera (Coherent, Beam-Code) to measure near-field

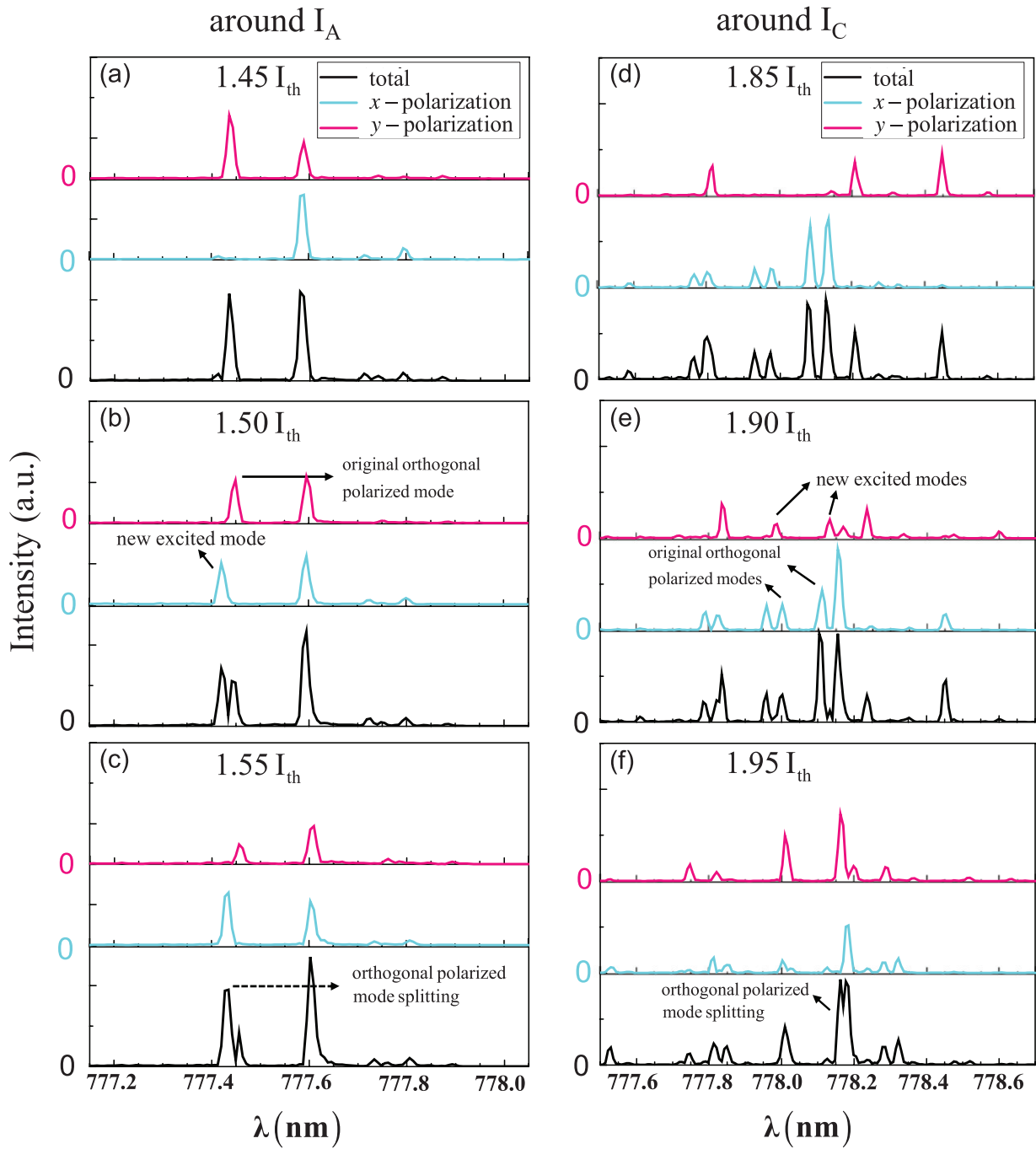


Figure 4. The variations of the optical spectra with the injected current near the kinks in the L-I curves for the two orthogonal polarized components.

patterns. The other part of the light was split into two orthogonal polarized lights by passing it through a polarization beam splitter (PBS) for further measurement. We identified the light as an *x*-polarized beam (*y*-polarized beam) whose direction of polarization was along the horizontal axis (vertical axis) of the device. The intensity time traces of the two orthogonal polarized beams were detected by a fast (1 GHz) oscilloscope. Lasing modes with different transverse orders could be generated via detuning the device temperature. The spectral information of the radiation output was measured by a high-resolution optical spectrum analyzer (Advantest Q8347) with a resolution of 0.002 nm.

3. Results and discussion

First of all, the VCSEL device was operated at room temperature. The spectrum of the spontaneous emission revealed the frequency detuning to be approximately 1.26 THz. It was experimentally found that the threshold currents I_{th} for both polarized components were nearly the same and approximately 17.8 mA. Figure 2 illustrates experimental results for the polarization resolved near-field patterns at the injected currents of $1.0 I_{th}$, $1.21 I_{th}$, $1.50 I_{th}$ and $1.85 I_{th}$. Just near lasing threshold, the lasing modes for both polarization components are accompanied by intense spontaneous emissions to cause

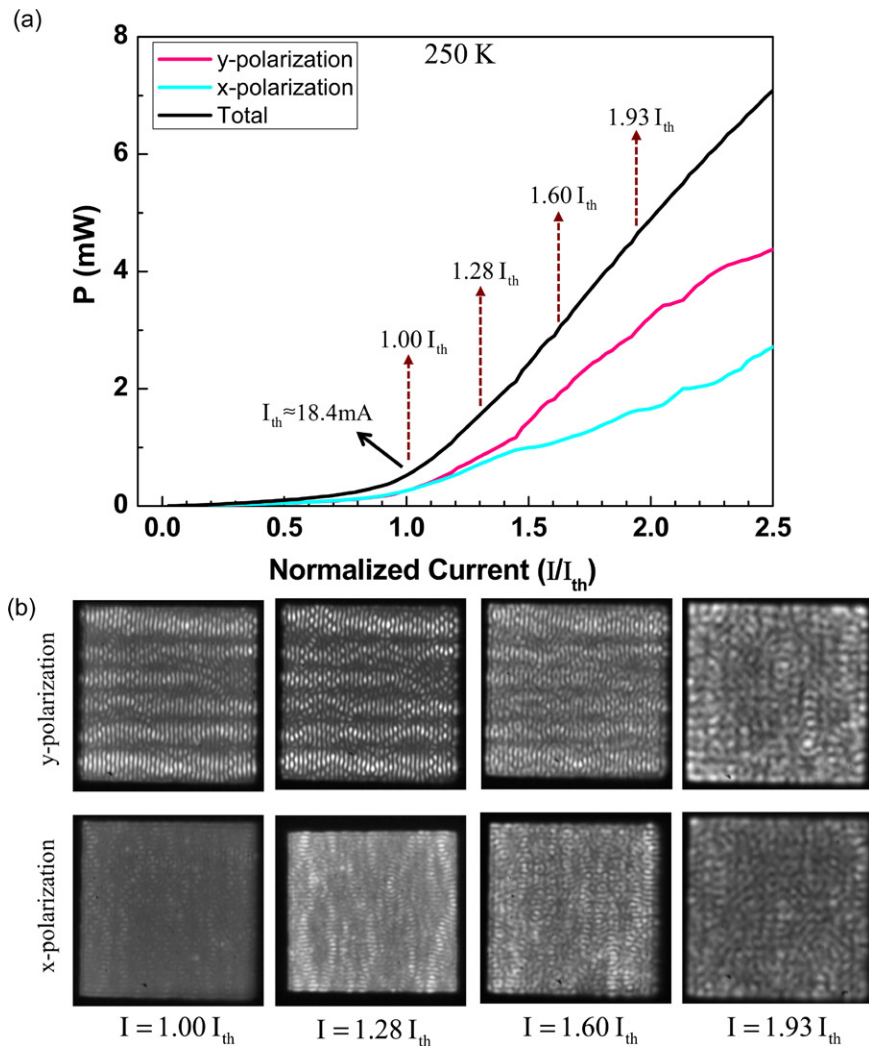


Figure 5. (a) The L-I curve in two orthogonal polarizations for the square-shaped VCSEL at the device temperature of 250 K. (b) The polarization resolved near-field patterns at different injection current.

the patterns to be ambiguous. At the case of $I = 1.21 I_{th}$, the lasing pattern for each polarization component can be found to become relatively sharp. Furthermore, the irregularly spatial morphologies imply that lasing modes are severely affected by thermal effects. When the injected current is further increased up to $I = 1.50 I_{th}$ or higher, the number of the lasing transverse modes gradually grows to turn the wave patterns into vagueness. Note that the lasing modes in the large-aperture device are considerably more than those in the small-aperture one. The lasing patterns also reveal that the transverse modes for the two orthogonally polarized components have notable spatial overlaps that could possibly lead to mode competition.

Figure 3(a) depicts the L-I curves for the two orthogonally polarized components. The slopes of the polarization resolved L-I curves can be seen to exhibit abrupt changes (kinks) when the injected current, with respect to the threshold current, I/I_{th} , is the values of 1.50, 1.65, 1.90 and 2.30. Figure 3(b) shows the time traces of the output powers for two orthogonal polarizations at the kinks of L-I curves. It is clear that the output powers of the two orthogonally polarized components display the phenomenon of anti-phase oscillation, which is a typical feature of polarization switching. The oscillation amplitude

of the anti-phase dynamics in the large-aperture device can be found to be relatively smaller than the observation in the small-aperture one. This result is due to the fact that in the large-aperture VCSEL, numerous lasing modes of the two orthogonally polarized components do not participate in the mode competition so as to contribute significant constant levels in the time traces. Figure 4 depicts the variations of the optical spectra with the injected current near the kinks in the L-I curves for the two orthogonally polarized components. It can be seen that the variations of the lasing modes for the two orthogonal polarizations are not synchronized, and the optical spectra exhibit a phenomenon of mode splitting.

Next the VCSEL device was operated at a temperature of 250 K to obtain a frequency detuning of 9.58 THz. The L-I curves for the two orthogonally polarized components are shown in figure 5(a). Unlike the results observed at room temperature, the kinks in the L-I curves are not conspicuous. Figure 5(b) depicts the experimental results for the polarization resolved near-field patterns at different injected currents. It can be seen that the lasing patterns generally display a structure of quasi-periodic linear ridges for the injected current below $1.60 I_{th}$. The structure of quasi-periodic linear

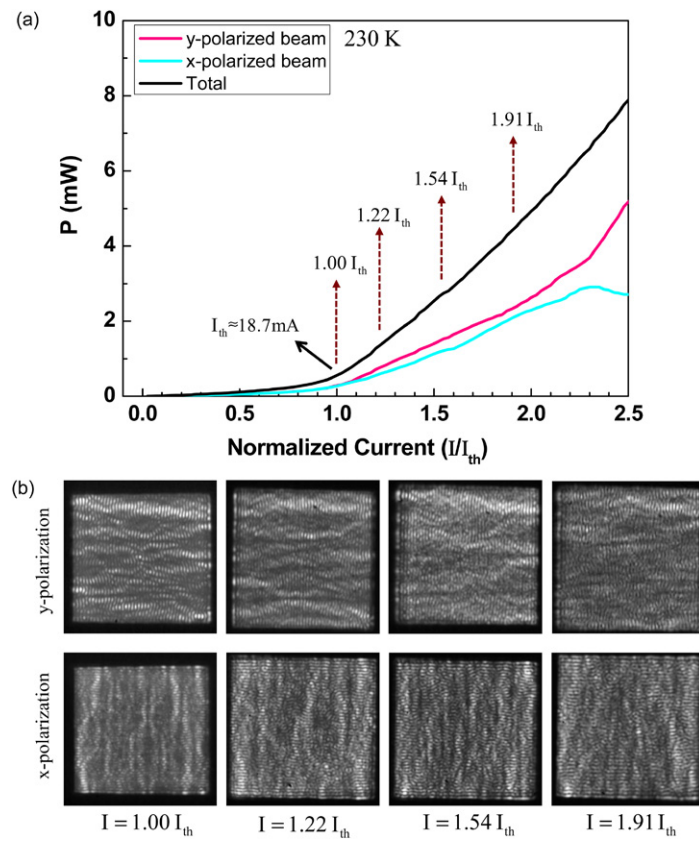


Figure 6. (a) The L-I curve in two orthogonal polarizations for the square-shaped VCSEL at the device temperature of 230 K. (b) The polarization resolved near-field patterns at different injection current.

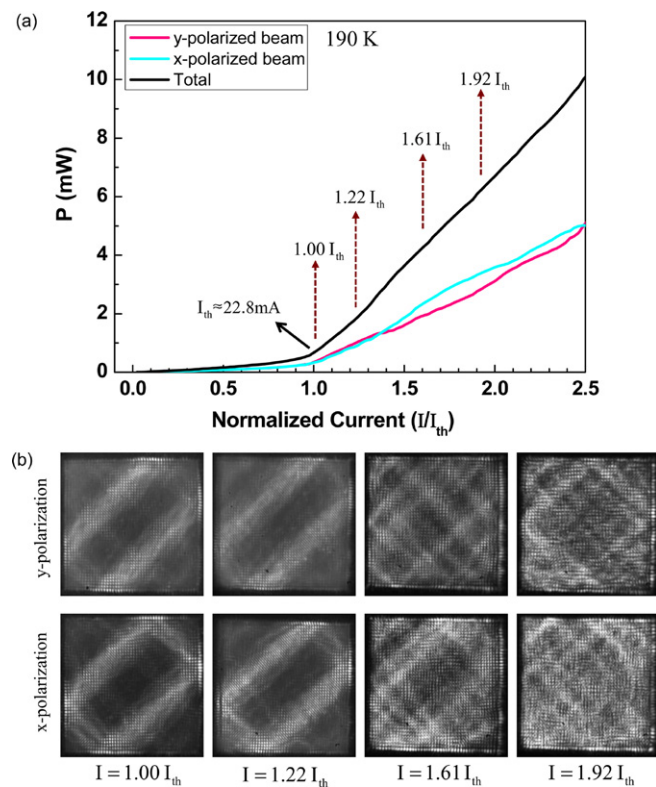


Figure 7. (a) The L-I curve in two orthogonal polarizations for the square-shaped VCSEL at the device temperature of 190 K. (b) The polarization resolved near-field patterns at different injection current.

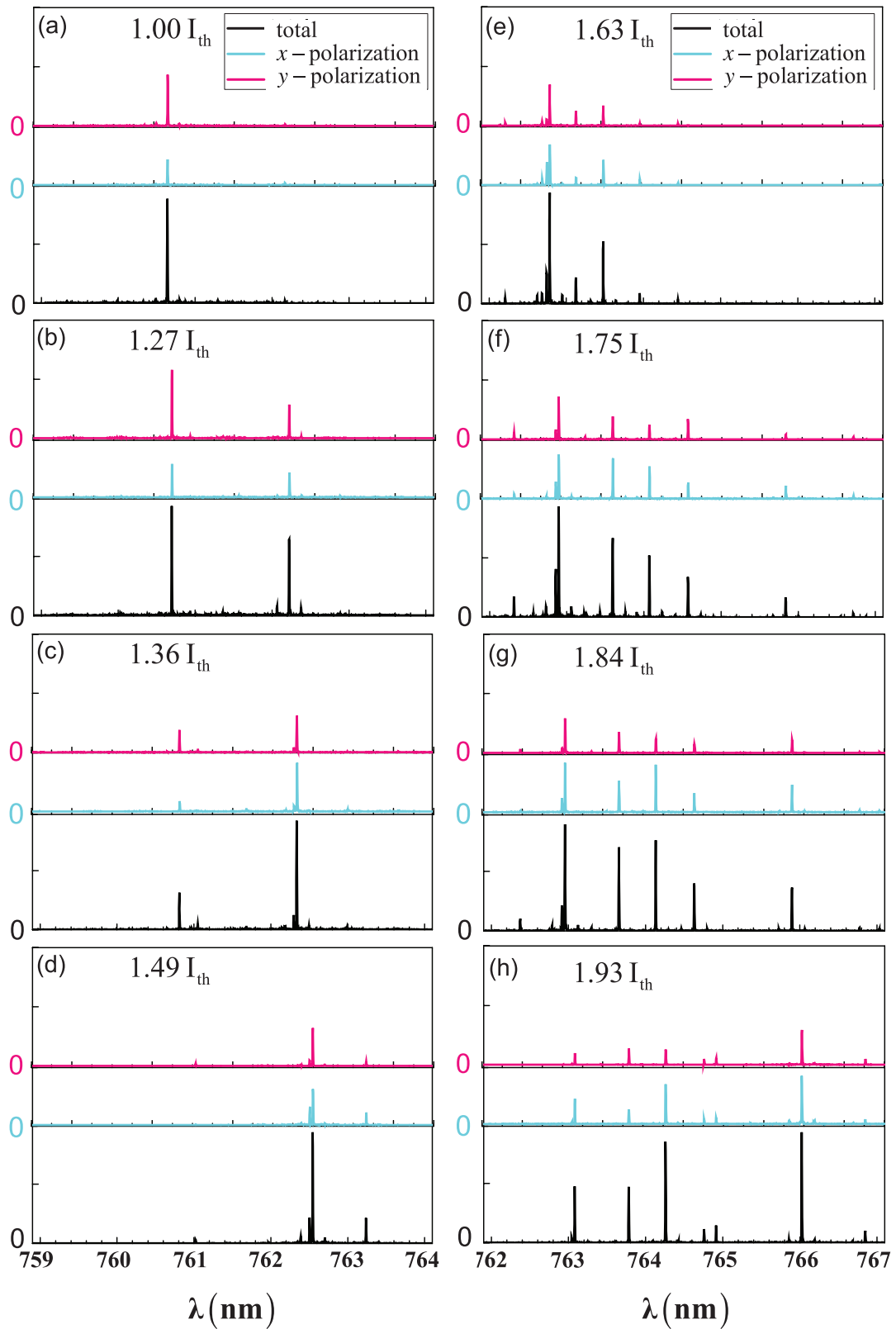


Figure 8. Polarization resolved optical spectra (blue and red lines respectively correspond to x - and y -polarized states) and total emitted optical spectra (black line) for the VCSEL operated at injected current of (a) $1.00 I_{th}$, (b) $1.27 I_{th}$, (c) $1.36 I_{th}$, (d) $1.49 I_{th}$, (e) $1.63 I_{th}$, (f) $1.75 I_{th}$, (g) $1.84 I_{th}$ and (h) $1.93 I_{th}$.

ridges could be theoretically reconstructed with the optical billiard model [22–24]. The laterally optical confinement of the VCSELs has been identified to come from the

oxide boundary. To be brief, the lasing transverse modes are mainly determined by lateral confinement instead of the thermal effect under the circumstances of low temperature

and large detuning. Based on the measured results from numerous samples, the polarization direction was found to be generally perpendicular to the linear ridge. Since the directions of linear ridges for both polarization components were almost orthogonal, the mode competition could be effectively avoided so as not to cause polarization switching. We also recorded the time traces to confirm that there was no obvious interaction oscillation between the two orthogonally polarized components. When the injected current was far above $I = 1.60 I_{th}$, more transverse modes were excited and the polarization resolved near-field patterns became rather vague, as shown in figure 5(b) for the case of $I = 1.93 I_{th}$. Subsequently, the VCSEL device was cooled to a temperature of 230 K to reach a frequency detuning of 17.7 THz. Figures 6(a) and (b) show the experimental results for the L-I curves and the polarization resolved near-field patterns for several injected currents. The overall behaviors were found to be similar to those shown in figures 5(a) and (b) for the experimental results observed at 250 K.

The operating temperature was then set at a temperature of 190 K and the frequency detuning was found to be approximately 32 THz. Figure 7(a) depicts the L-I curves for the two orthogonally polarized components at 190 K. Once again, there are no noticeable kinks in the polarization-resolved L-I curves, and there is no obvious polarization switching to be observed. Figure 7(b) shows the experimental results for the near-field patterns at different injected currents. It is found that the lasing modes for both polarizations are prominently localized on the ray paths of the diamond structure for the injected current below $1.30 I_{th}$. The lasing mode concentrated on the diamond trajectory was nicely reconstructed in the earlier investigation with the model of wave billiards [22–24]. When the injected current is higher than $I = 1.30 I_{th}$, as shown in figure 7(b), the lasing modes are localized on the intricate trajectories corresponding to the multiple diamond structure. Figure 8 depicts the experimental results for the optical spectra of the lasing modes along the two orthogonal polarizations at numerous injected currents from lasing threshold to $I/I_{th} = 2.0$. Figure 8(a) reveals that at the near lasing threshold the orthogonally polarized components are locked in a single frequency. When the injected currents are between $1.2 I_{th}$ and $1.5 I_{th}$, the orthogonally polarized modes are also synchronized and generally belong to the two-frequency operation, as shown in figures 8(b)–(d). For injected currents greater than $1.6 I_{th}$, the mode numbers for both orthogonally polarized components are found to increase rapidly. Despite more and more lasing modes, the wavelength components for the two orthogonally polarized modes are still utterly identical and display an excellent frequency locking, as seen in figures 8(e)–(h). The total frequency locking between two orthogonal polarization components makes the devices immune to polarization switching.

Finally, experimental results revealed that lowering the operating temperature to below 190 K would cause the lasing threshold to rapidly increase and could not achieve a higher-frequency detuning. In other words, frequency detuning at 190 K was almost the maximum value of the present device.

The range of the frequency detuning is limited by the effective optical confinement of the oxide boundary.

4. Conclusions

In conclusion, we have used cryogenic cooling to explore the polarization characteristics of broad-area square-shaped VCSELs in a wide range of frequency detuning. We found that lasing modes were primarily subject to thermal effects at room temperature and turned to be controlled by the oxide confinement for operating temperature below 260 K. Under the thermally controlled regime, there was obvious polarization switching to be observed. In contrast, there was no conspicuous polarization switching to be observed under the boundary-controlled regime. It was remarkably found that the two orthogonally polarized components were persistently locked in the same spectral components from single-mode to multi-mode operation; even the injected current increased to far above lasing threshold. The total frequency locking leads the device to be immune against polarization switching.

The authors thank the National Science Council for their financial support of this research under Contract No. MOST 103-2112-M-009-016-MY3.

References

- [1] Panjotov K, Berghmans F, Peeters M, Verschaffelt G, Danckaert J, Veretennicoff I and Thienpont H 1999 Data transparent reconfigurable optical interconnections using polarization switching in VCSEL's induced by optical injection *IEEE Photon. Technol. Lett.* **11** 985–7
- [2] Hudgings J A, Lim S F, Li G S, Yuen W, Lau K Y and Chang-Hasnain C J 1999 Compact, integrated optical disk readout head using a novel bistable vertical-cavity surface-emitting laser *IEEE Photon. Technol. Lett.* **11** 245–7
- [3] Geske J, Jayaraman V, Goodwin T, Culick M, MacDougal M, Goodnough T, Welch D and Bowers J E 2000 2.5 Gb s⁻¹ Transmission over 50 km with a 1.3 μm vertical-cavity surface-emitting laser *IEEE Photon. Technol. Lett.* **12** 1707–9
- [4] Oikawa Y, Hasegawa H, Suzuki K, Inoue Y, Hirooka T and Nakazawa M 2007 4 × 10 Gb s⁻¹ WDM transmission over a 5 km-long photonic crystal fiber in the 800 nm region *IEEE Photon. Technol. Lett.* **19** 613–5
- [5] van Exter M P, Willemsen M B and Woerdman J P 1998 Polarization fluctuations in vertical-cavity semiconductor lasers *Phys. Rev. A* **58** 4191–205
- [6] van Exter M P, van Doorn A K J and Woerdman J P 1998 Electro-optic effect and birefringence in semiconductor vertical-cavity lasers *Phys. Rev. A* **56** 845–53
- [7] van Doorn A K J, van Exter M P and Woerdman J P 1998 Strain-induced birefringence in vertical-cavity surface-emitting semiconductor lasers *IEEE J. Quantum Electron.* **34** 700–6
- [8] Panajotov K, Ryvkin B, Danckaert J, Peeters M, Thienpont H and Veretennicoff I 1998 Polarization switching in VCSEL's due to thermal lensing *IEEE Photon. Technol. Lett.* **10** 6–8
- [9] Knopp K J, Christensen D H, Rhodes G V, Pomeroy J M, Goldberg B B and Ünlü M S 1999 Spatio-spectral mapping of multimode vertical cavity surface emitting lasers *J. Light. Technol.* **17** 1429–5

- [10] Choquette K D, Richie D A and Leibenguth R E 1994 Temperature dependence of gain-guided vertical-cavity surface emitting laser polarization *Appl. Phys. Lett.* **64** 2062–4
- [11] Choquette K D, Schneider R P, Lear K L Jr and Leibenguth R E 1995 Gain-dependent polarization properties of vertical-cavity lasers *IEEE J. Sel. Top. Quantum Electron.* **1** 661–6
- [12] Regalado J M, Chilla J L A, Rocca J J and Brusenbach P 1997 Polarization switching in vertical-cavity surface emitting lasers observed at constant active region temperature *Appl. Phys. Lett.* **70** 3350–2
- [13] Sondermann M, Weinkath M and Ackemann T 2003 Two-frequency emission and polarization dynamics at lasing threshold in vertical-cavity surface-emitting lasers *Phys. Rev. A* **68** 033822
- [14] Olejniczak L, Panajotov K, Thienpont H, Sciamanna M, Mutig A, Hopfer F and Bimberg D 2011 Polarization switching and polarization mode hopping in quantum dot vertical-cavity surface-emitting lasers *Opt. Express* **19** 2476–84
- [15] Hong Y, Spencer P S and Shore K A 2004 Suppression of polarization switching in vertical-cavity surface-emitting lasers by use of optical feedback *Opt. Lett.* **29** 2151–3
- [16] Arizaleta Arteaga M, Parriaux O, López-Amo M, Thienpont H and Panajotov K 2007 Polarized optical feedback from an extremely short external cavity for controlling and stabilizing the polarization of vertical cavity surface emitting lasers *Appl. Phys. Lett.* **90** 121104
- [17] Panajotov K, Nagler B, Verschaffelt G, Georgievski A, Thienpont H, Danckaert J and Veretennicoff I 2000 Impact of in-plane anisotropic strain on the polarization behavior of vertical-cavity surface-emitting lasers *Appl. Phys. Lett.* **77** 1590–2
- [18] Chu H Y, Yoo B S, Park M S and Park H H 1997 Polarization characteristics of index-guided surface-emitting lasers with tilted pillar structure *IEEE Photon. Technol. Lett.* **9** 1066–8
- [19] Choquette K D and Leibenguth R E 1994 Control of vertical-cavity laser polarization with anisotropic transverse cavity geometries *IEEE Photon. Technol. Lett.* **6** 40–2
- [20] Wang W, Ning Y Q, Zhang J L, Qin L, Zeng Y G, Liu Y, Tong C Z and Wang L J 2012 Power and spectra polarization of large-aperture rectangular-shaped vertical-cavity top-emitting lasers *Laser Phys.* **22** 554–8
- [21] Tan M P, Kasten A M, Strand T A and Choquette K D 2012 Polarization switching in vertical-cavity surface-emitting lasers with anisotropic cavity geometry and injection *IEEE Photon. Technol. Lett.* **24** 745–7
- [22] Huang K F, Chen Y F, Lai H C and Lan Y P 2002 Observation of the wave function of a quantum billiard from the transverse patterns of vertical cavity surface emitting lasers *Phys. Rev. Lett.* **89** 224102
- [23] Chen Y F, Huang K F and Lai H C 2003 Rules of selection for spontaneous coherent states in mesoscopic systems: using the microcavity laser as an analog study *Phys. Rev. E* **68** 026210
- [24] Chen C C, Su K W, Chen Y F and Huang K F 2008 Various high-order modes in vertical-cavity surface-emitting lasers with equilateral triangular lateral confinement *Opt. Lett.* **33** 509–11
- [25] Babushkin I V, Schulz-Ruhtenberg M, Loiko N A, Huang K F and Ackemann T 2008 Coupling of polarization and spatial degrees of freedom of highly divergent emission in broad-area square vertical-cavity surface-emitting lasers *Phys. Rev. Lett.* **100** 213901
- [26] Hegarty S P, Huyet G, McInerney J G and Choquette K D 1999 Pattern formation in the transverse section of a laser with a large fresnel number *Phys. Rev. Lett.* **82** 1434–7